Electronic Supplementary Material (ESI) for Materials Horizons.
This journal is © The Royal Society of Chemistry 2022

Supporting information

Near-Infrared Polarization-Sensitive Photodetection via Interfacial Symmetry Engineering of Si/$MAPbI_3$ Heterostructural Single Crystal

Jianbo Wu[a, b], Xinyuan Zhang[a, b], Ziyang Wang[a], Lishan Liang[a], Xinyi Niu[a], Qianwen Guan[a, b], Shihai You[a], and Junhua Luo*[a, b, c]

a J. Wu, X. Zhang, Z. Wang, L. Liang, X. Niu, Q. Guan, S. You, Prof. J. Luo
State Key Laboratory of Structural Chemistry
Fujian Institute of Research on the Structure of Matter, Chinese Academy of Sciences
Fuzhou, Fujian 350002, P. R. China
E-mail: jhluo@fjirsm.ac.cn

b J. Wu, X. Zhang, Q. Guan, Prof. J. Luo
University of Chinese Academy of Sciences
Beijing 100049, P. R. China

c Prof. J. Luo
School of Chemistry and Chemical Engineering
Jiangxi Normal University
Nanchang, Jiangxi 330022, P. R. China

Experimental Section

Materials: The materials used were lead iodide (PbI_2, Aladdin Chemistry Co., Ltd., 99.9%), methylamine iodide (MAI, self-synthesized), γ-butyrolactone (GBL, Shanghai Tichem Chemical Co., Ltd, 99.8%), (3-aminopropyl)triethoxysilane (APTES, Aladdin Chemistry Co., Ltd., >99%), 1,2-dichlorobenzene (DCB, Aladdin Chemistry Co., Ltd., >99%), hydroiodic acid (HI, Aladdin Chemistry Co., Ltd., 48% wt/wt aq), 2-propanol (IPA, Aladdin Chemistry Co., Ltd., >99.5%)

Preparation of the precursor solutions: The raw materials 2.305 g PbI_2 and 0.795 g MAI were dissolved in 5 mL GBL solvent. A bright-yellow solution was obtained.

Growth of $MAPbI_3$ single crystal: $MAPbI_3$ single crystals were grown via inverse-temperature crystallization method. The precursor solution was transferred to a vial and then heat up to 100℃ in oil bath and maintained hours under this temperature for the growth of the single crystal.

Preparation of modified Si substrate: The method of modifying Si substrate was in accordance with the previous report. The precleaned Si (n-type) wafer was placed into a mixture of DCB and APTES solvent (20:1) for 12 h at 50 °C and ultrasonically rinsed with IPA to obtain NH_2-terminatedmolecules on the surface. The wafer was then treated with HI (aq.) to convert the amino groups into $–NH_3I$ groups.

Growth of Si-integrated $MAPbI_3$ single crystal: A small droplet of the $MAPbI_3$/GBL solution was dropped onto the modified Si wafer. Then, the Si wafer with small droplet was heat to 50℃ to volatilize the solvent and obtain the seed crystal. After that, the Si wafer with the seed crystal was placed into the preheat $MAPbI_3$/GBL solution for the growth of the Si-integrated $MAPbI_3$ single crystal. The solution was heated to 100 °C and maintained this temperature for hours.

Powder X-ray diffraction: Powder X-ray diffraction measurement was performed on a Rigaku MiniFlex 600 diffractometer at atmosphere environment. The diffraction patterns were collected in the 2θ range of 5°–50° with a step size of 0.5°/min.

Scanning electron microscope measurement (SEM): The SEM image was collected on ZEISS Sigma 300 field-emission scanning electron microscope operated at 3kV.

Absorption spectrum measurement: Absorption spectrums of $MAPbI_3$ was performed on a Perkin-Elmer Lambda 900 UV–Vis–NIR spectra photometer at room temperature. In which $BaSO_4$ was used as the 100% reflectance reference.

Photoluminescence spectra measurements: Emission spectra of $MAPbI_3$ and the $MAPbI_3$/Si heterojunction were performed on an Edinburgh FLS1000 fluorescence spectrometer. The lifetime of $MAPbI_3$ and the $MAPbI_3$/Si heterojunction were measured on an Edinburgh FLS1000 fluorescence spectrometer using a picosecond pulsed diode laser. The dynamics of emission decay were monitored by using the FLS1000's time-correlated single-photon counting capability (1,024 channels; 500 ns window) with data collection for 10,000 counts in the maximum channel.

Optoelectronic performances measurements: The current vs voltage (I–V) and photocurrent vs time (I–t) with light on and off (measured at zero bias) were measured using a high precision electrometer (Keithley 6517B). I–V tests were collected under the 405 nm, 520 nm, 637 nm and 785 nm continuous-wave lasers (ITC4001). I–t was collected under the 785 nm continuous-wave lasers (ITC4001). The incident light intensity was measured by light power meter.

Results and Discussion

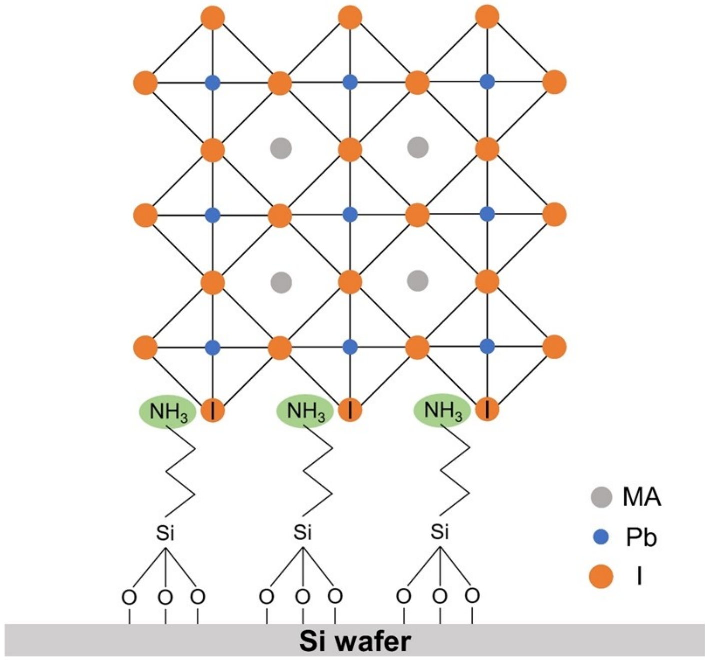

Figure S1. Schematic of the $MAPbI_3$/Si heterostructure

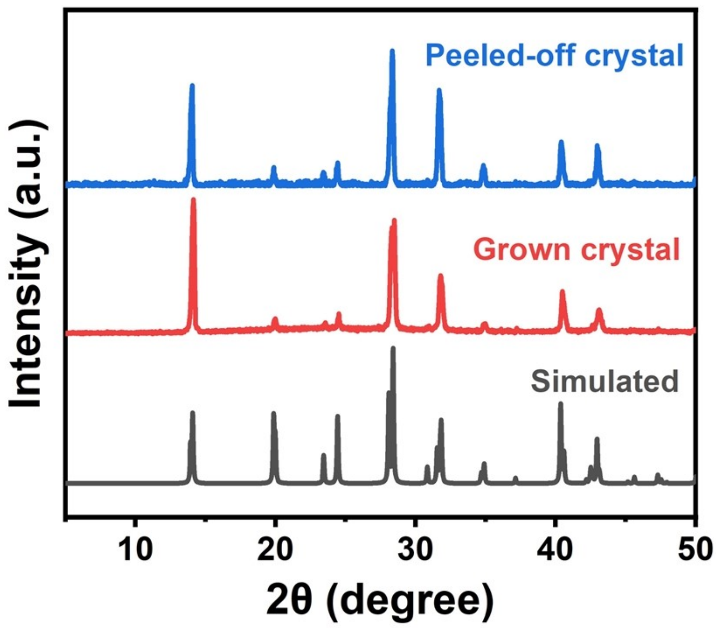

Figure S2. PXRD patterns of the simulation of $MAPbI_3$ crystal, naturally grown crystal, and the peeled-off $MAPbI_3$ crystal from the Si wafer.

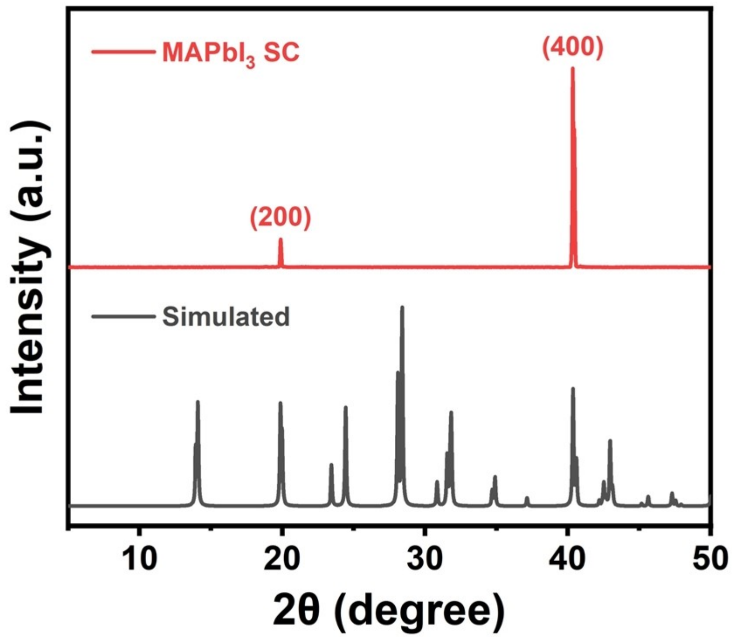

Figure S3. XRD pattern of the $MAPbI_3$ single crystal.

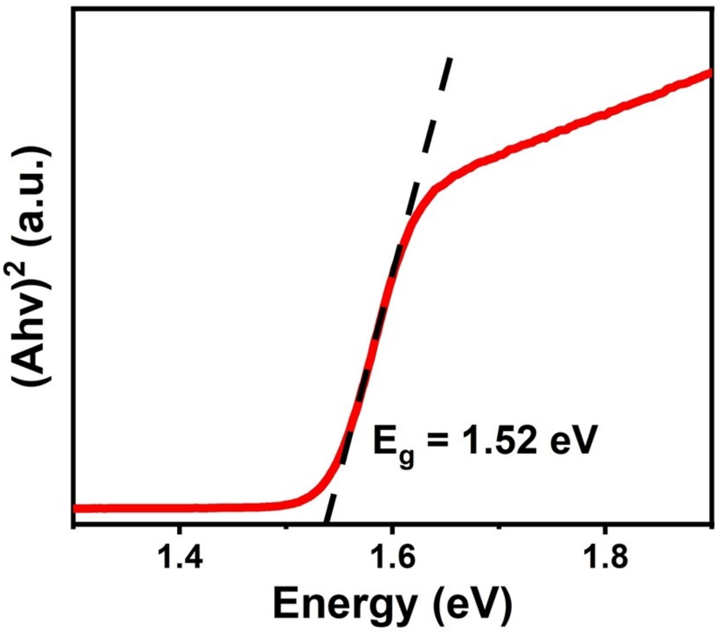

Figure S4. The calculation of $MAPbI_3$ optical band gap via corresponding Tauc plots.

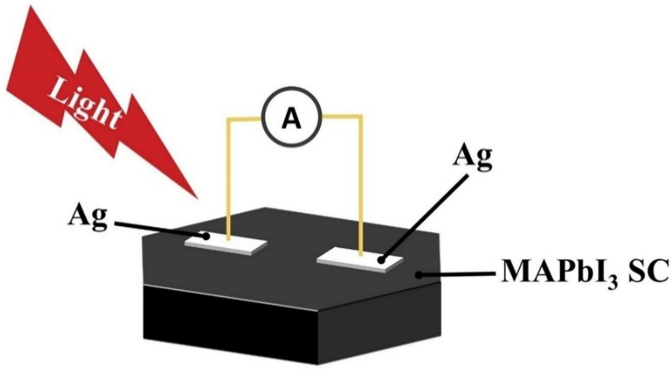

Figure S5. Schematic illustration of the $MAPbI_3$ SC device.

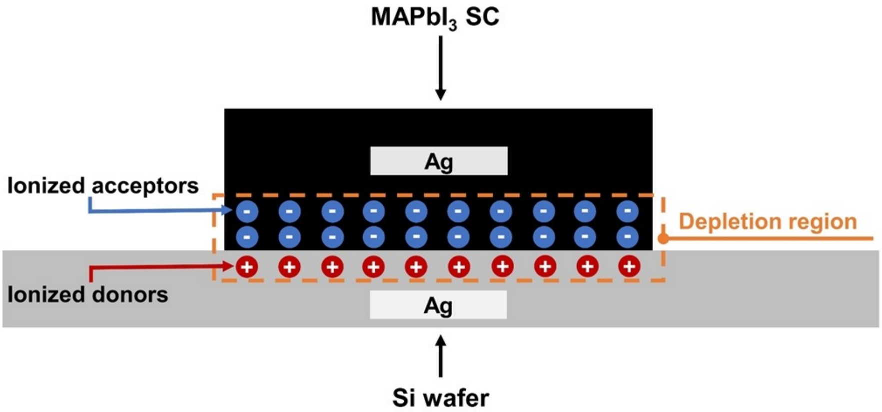

Figure S6. A schematic of depletion region at the $MAPbI_3$/Si heterostructure interface

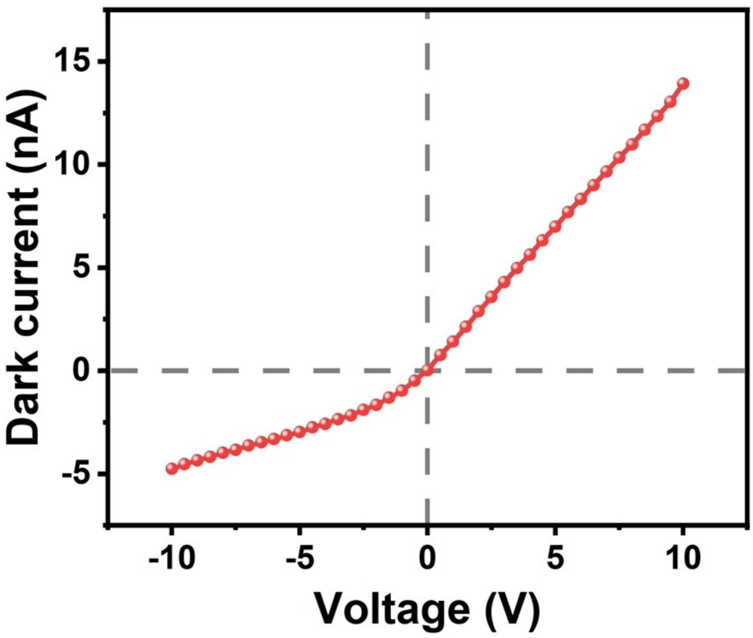

Figure S7. Dark current of the heterojunction photodetector

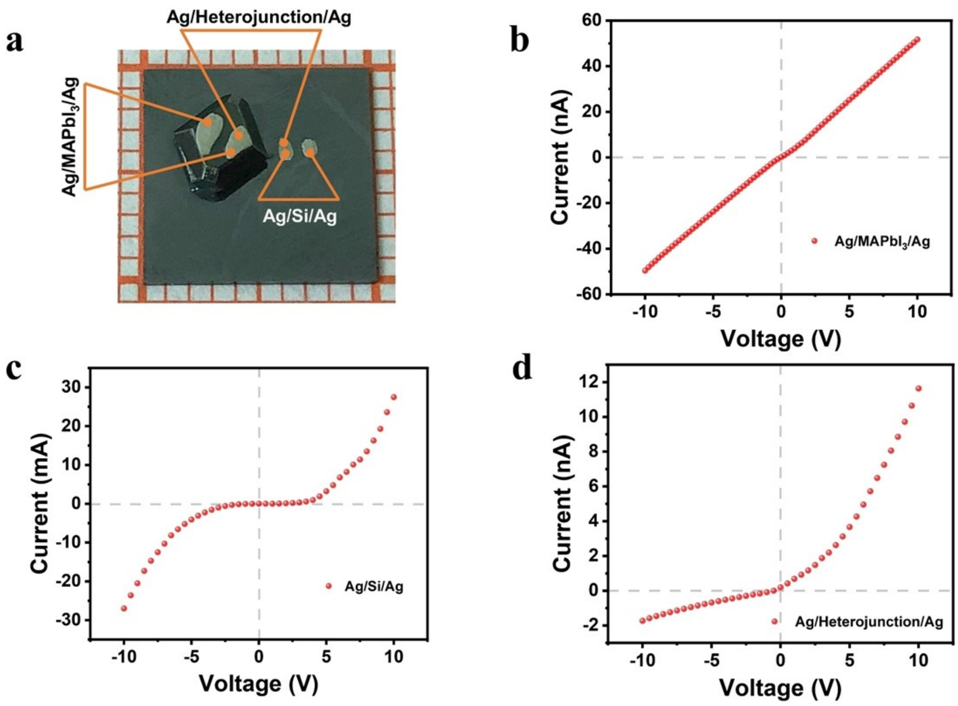

Figure S8. (a) Photograph of Ag/$MAPbI_3$/Ag, Ag/Si/Ag and Ag/Heterojunction/Ag device in the same heterostructure sample. (b) *I-V* curve of Ag/$MAPbI_3$/Ag under the dark condition. (c) *I-V* curve of Ag/Si/Ag under the dark condition. (d) *I-V* curve of Ag/Heterojunction/Ag under the dark condition.

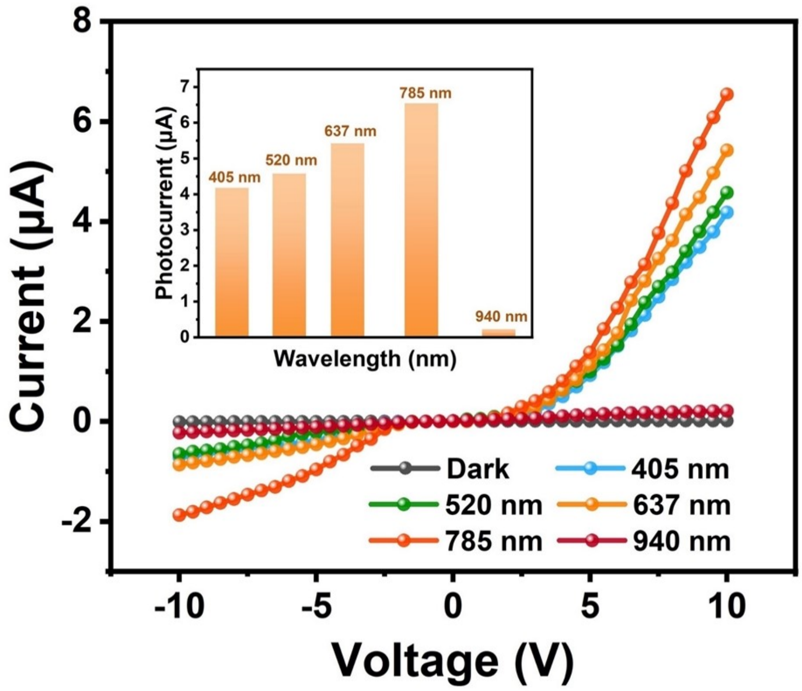

Figure S9. *I−V* curves of the heterojunction photodetector under the different wavelength illumination at the power density of 19.4 mW/cm^2. The insert shows the photocurrents of the heterojunction device as a function of wavelength.

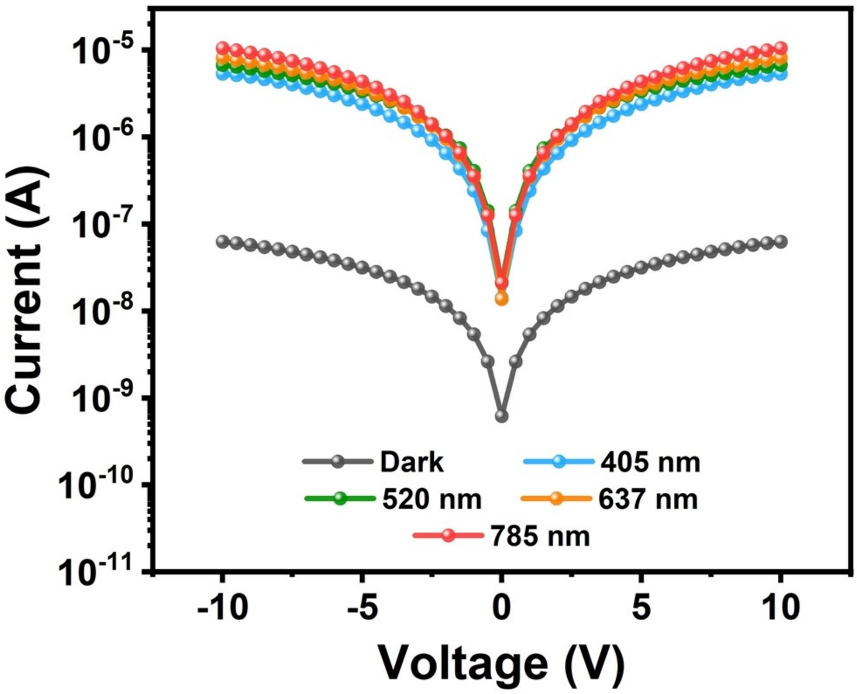

Figure S10. *I*–*V* curves of the $MAPbI_3$ SC photodetector under the different wavelength illumination at the power density of 19.4 mW/cm^2.

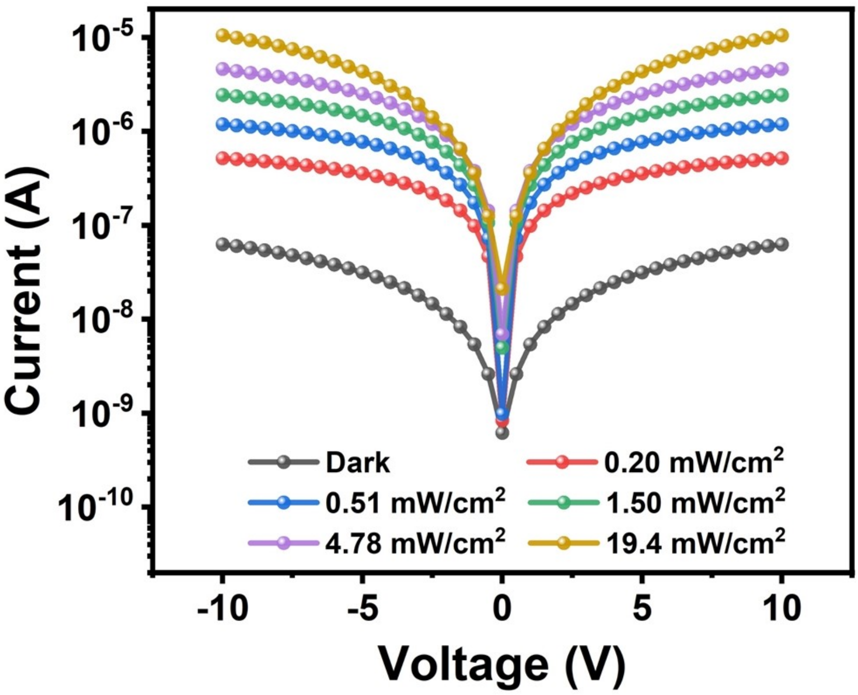

Figure S11. *I*–*V* curves of the $MAPbI_3$ SC photodetector under the 785 nm illumination with different power density.

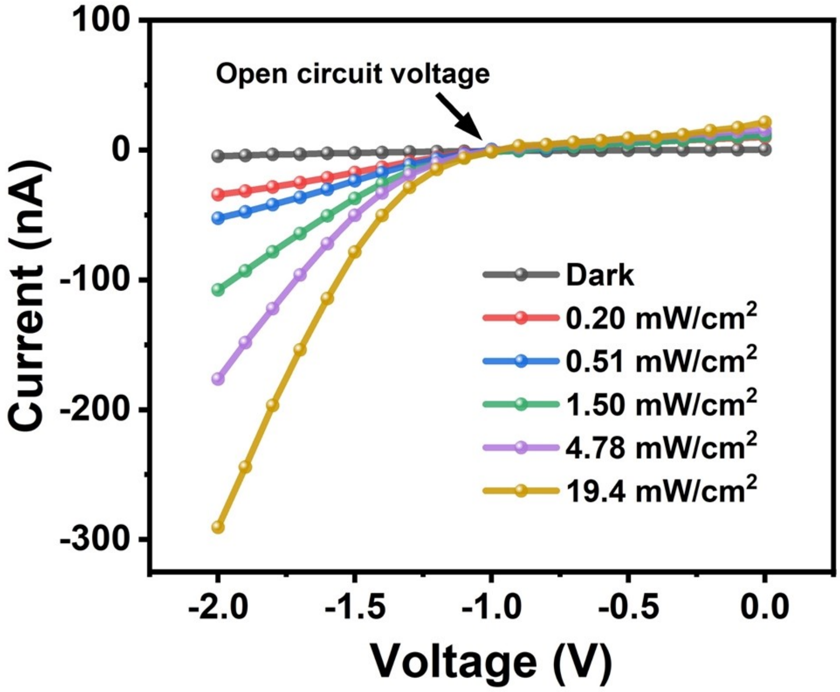

Figure S12. Open-circuit voltage of the heterojunction device.

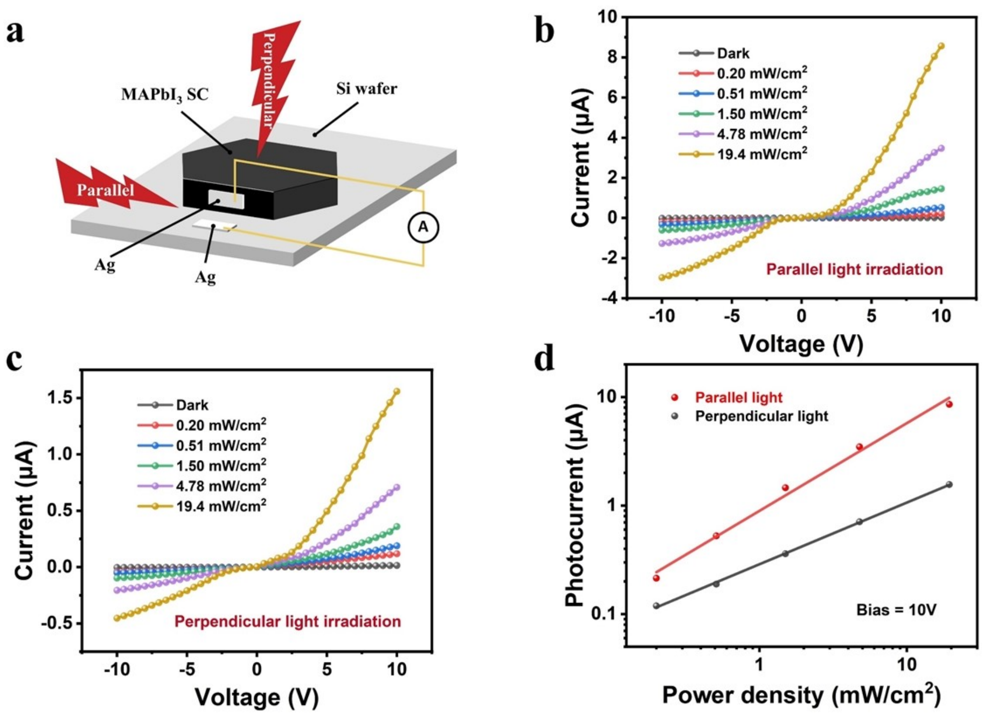

Figure S13. (a) Schematic illustration of the $MAPbI_3$/Si heterostructure photodetector with different incident directions. (b) *I-V* curves of heterostructure photodetector with parallel light irradiation. (c) *I-V* curves of heterostructure photodetector with perpendicular light irradiation. (d) Light power density dependent photocurrent with different incident directions.

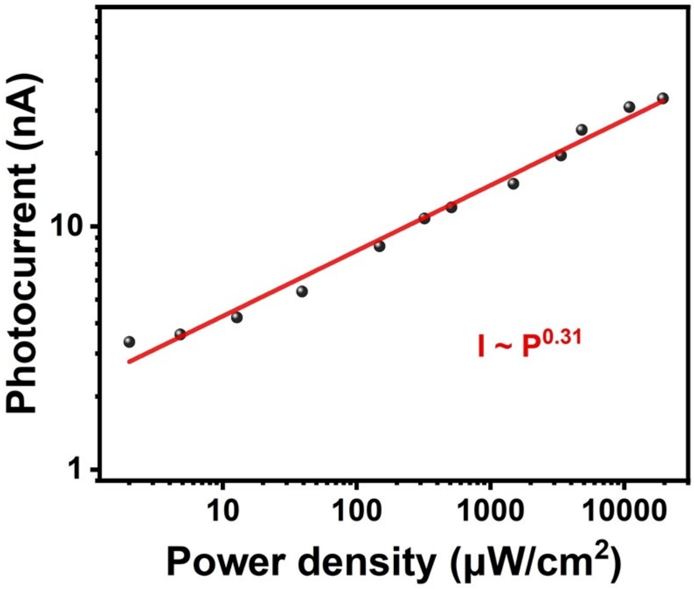

Figure S14. Light power density dependent photocurrent of the $MAPbI_3$/Si device under the self-driven mode.

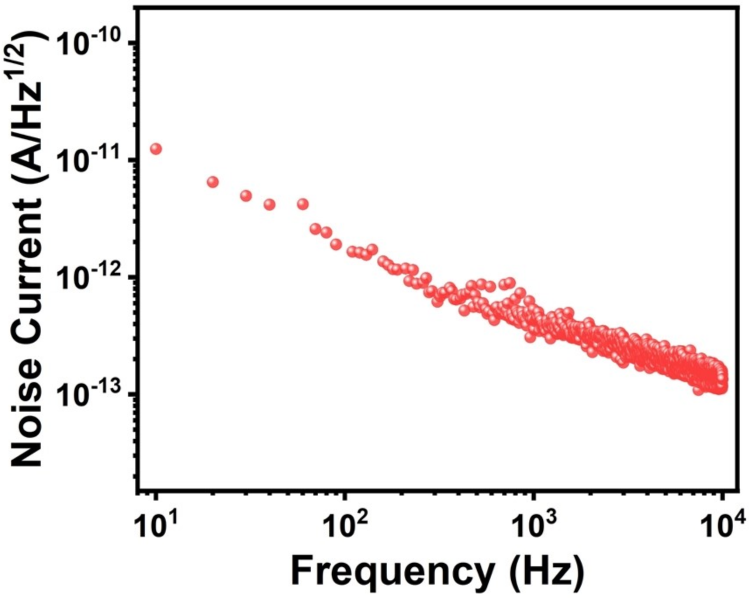

Figure S15. The current noise power spectra at 0 V bias.

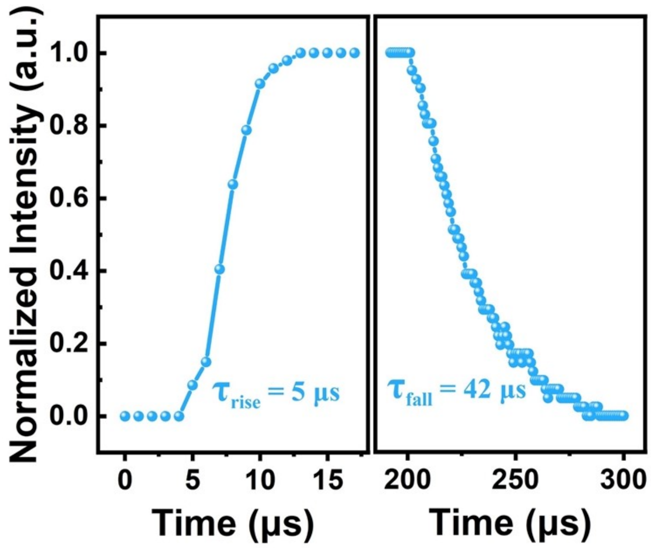

Figure S16. The response time of the heterojunction photodetector under the self-powered mode at 785 nm.

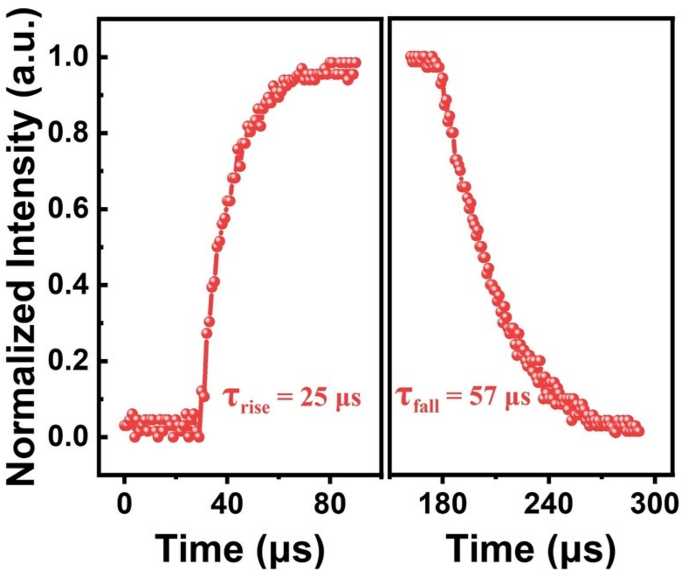

Figure S17. The response time of the heterojunction photodetector under the self-powered mode at 940 nm.

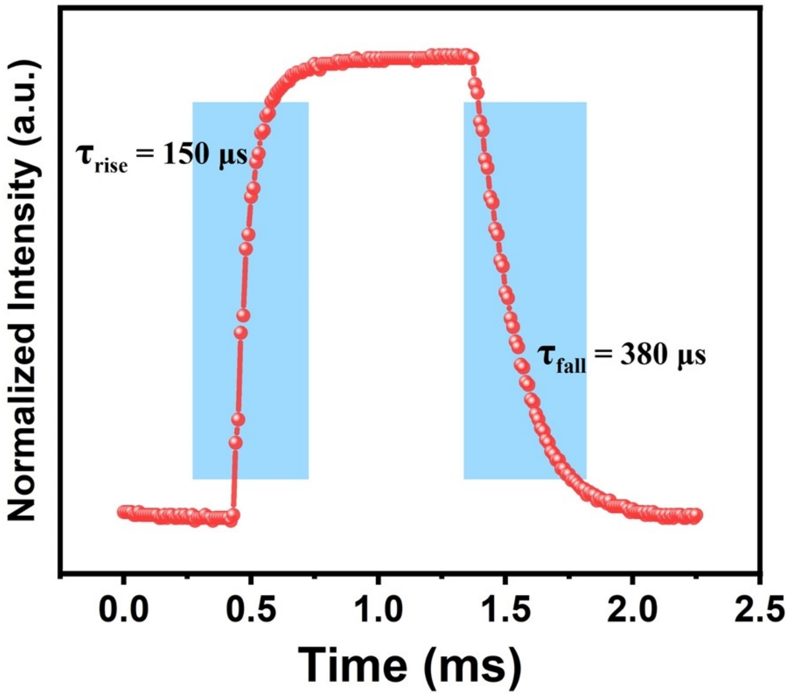

Figure S18. The response time of the $MAPbI_3$ SC photodetector under 10 V bias at 785 nm.

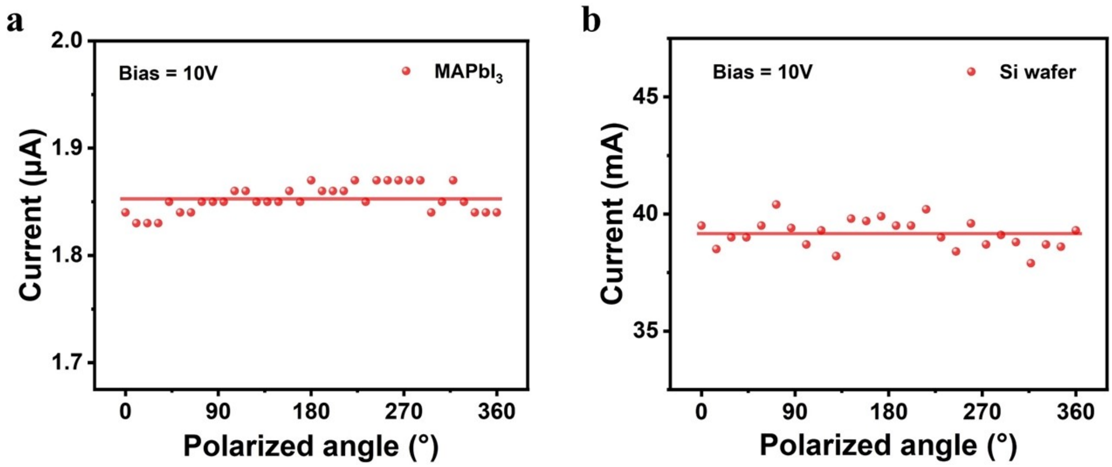

Figure S19. Polarized photocurrent of the pure (a) $MAPbI_3$ and (b) Si.

Table S1. Performance comparison of $MAPbI_3$/Si heterojunction NIR polarization-sensitive photodetector with other devices.

Devices	λ (nm)	D^* (Jones)	Polarized ratio	Condition	Ref.
$MAPbI_3$/Si	405-940	7.35×10^{12}	2.8 @ 940 nm 3.3 @ 785 nm	Self-powered	This work
$MAPbI_3$ single crystal	275-790	-	-	1 V	1
$MAPbI_3$/graphene	260-900	4.5×10^{11}	-	Self-powered	2
$MAPbI_3$/PDPP3T	300-937	1.5×10^{10}	-	1 V	3
PTAA/$MAPbI_3$/C_{60}/BCP	350-800	7.8×10^{12}	-	0.1 V	4
$MAPbI_3$ nanocrystal	400-980	1.77×10^{13}	-	Self-powered	5
$MAPbI_3$ nanoribbon	300-800	8.21×10^{11}	1.44 @ white light	2 V	6
$MAPbI_3$ nanowires	530	2×10^{13}	1.3 @ 530 nm	1 V	7
$MAPbI_3$ needlecrystal	405	-	1.57 @ 405 nm	5 V	8
$MAPbI_3$ nanowires	200-1000	4.73×10^{12}	2.2 @ 520 nm	1 V	9

References

1 Z. Lian, Q. Yan, Q. Lv, Y. Wang, L. Liu, L. Zhang, S. Pan, Q. Li, L. Wang, J. L. Sun, *Sci. Rep.* **2015**, *5*, 16563-16573.

2 J. Li, S. Yuan, G. Tang, G. Li, D. Liu, J. Li, X. Hu, Y. Liu, J. Li, Z. Yang, S. F. Liu, Z. Liu, F. Gao, F. Yan, *ACS Appl. Mater. Interfaces* **2017**, *9*, 42779-42787.

3 S. Chen, C. Teng, M. Zhang, Y. Li, D. Xie, G. Shi, *Adv. Mater.* **2016**, *28*, 5969-5974.

4 L. Shen, Y. Fang, D. Wang, Y. Bai, Y. Deng, M. Wang, Y. Lu, J. Huang, *Adv. Mater.* **2016**, *28*, 10794-10800.

5 C. Perumal Veeramalai, S. Yang, R. Zhi, M. Sulaman, M. I. Saleem, Y. Cui, Y. Tang, Y. Jiang, L. Tang, B. Zou, *Adv. Opt. Mater.* **2020**, *8*, 2000215-2000224.

6 S. Lim, M. Ha, Y. Lee, H. Ko, *Adv. Opt. Mater.* **2018**, *6*, 1800615-1800624.

7 L. Gao, K. Zeng, J. Guo, C. Ge, J. Du, Y. Zhao, C. Chen, H. Deng, Y. He, H. Song, G. Niu, J. Tang, *Nano Lett.* **2016**, *16*, 7446-7454.

8 Z. Zhao, Y. Li, Y. Du, L. Zhang, J. Wei, F. Lin, *ACS Appl. Mater. Interfaces* **2020**, *12*, 44248-44255.

9 R. Huang, D.-H. Lin, J.-Y. Liu, C.-Y. Wu, D. Wu, L.-B. Luo, *Sci. China Mater.* **2021**, *64*, 2497-2506.